JOURNAL OF MATERIALS SCIENCE 33 (1998) 5581–5588

Modulated-temperature differential scanning calorimetry and Raman spectroscopy studies of As_xS_{100-x} glasses

T. WAGNER, S. O. KASAP
Electronic Materials Research Laboratories, Department of Electrical Engineering, University of Saskatchewan, Saskatoon, S7N 5A9 Canada
E-mail: kasap@engr.usak.ca

M. VLCEK, A. SKLENÁR, A. STRONSKI
Department of General and Inorganic Chemistry, University of Pardubice, Pardubice 532 10, Czech Republic

Thermal properties of chalcogenide As_xS_{100-x} glasses in the glass transition region have been studied by modulated-temperature differential scanning calorimetry (MTDSC). All samples in this work were given the same thermal history by heating to a temperature above the glass transition, equilibrating and then cooling at a rate of 5 °C/min to a temperature of 20 °C. The reversing and non-reversing heat flows through the glass transformation region during both heating and cooling schedules were measured and the values of the parameters T_g, ΔH, C_p and ΔC_p, which characterize the thermal events in the glass transition region, were determined as a function of the glass composition. The structurally determined parameters T_g, ΔH, C_p and ΔC_p reveal major extrema when the composition of As_xS_{100-x} glass becomes $As_{40}S_{60}$, that is the same as the composition of the corresponding stoichiometric compound. In addition, we observe "small thresholds" in these properties at 28.5 at % As ($As_{28.5}S_{71.5}$) around the same composition as that reported in the As-Se glasses. No such thermal analysis had been done on the As_xS_{100-x} glasses previously. It is shown that As_xS_{100-x} glasses where $x < 25$ at % As are formed from two glass phases. From MTDSC measurements, it was possible to establish the probable composition of the high temperature glass phase and from Raman spectroscopy it was possible to correlate the MTDSC results with the structure of the As-S glasses.

1. Introduction

The Modulated-Temperature Differential Scanning Calorimetry (MTDSC) is a relatively new technique [1] that has been found to be a very powerful tool for accurately measuring the temperatures and enthalpies of various transitions occurring in a material. Recent applications of MTDSC has shown that it can be very useful for the interpretation of thermal properties, such as the heat capacity, in relation to the structure as, for example, in the case of chalcogenide glasses As-Se [2] Se-Te [3], Ge-Se [4, 5, 6], $Ge_xAs_yS_{60}$ [7], Ge-S [5, 6]. The aim of this work was to try to extend our conclusions for As-Se glasses [2] to the As-S chalcogenide glass system, with support of Raman spectroscopy as a direct tool towards establishing the structure of As-S glasses.

We carried out MTDSC measurements on a range of As-S glasses ($As_{10}S_{90}$ to $As_{42}S_{58}$) to obtain the reversing and non-reversing heat flows through the glass transition region both during heating and cooling schedules. All measurements were carried out on samples that were given the same thermal history to ensure meaningful comparisons between samples. All cooling schedules were started from a temperature above the glass transition region so that the samples were cooled from the liquid-like equilibrium state. We compare our MTDSC results with previously published works on glass transition in As-S glasses and also discuss the results in terms of recent structural models for chalcogenide glasses. We were motivated in studying the As-S glasses due to the interesting structural properties of these chalcogenide glasses [5, 8–14] and current and potential uses of As-S in various imaging and optical applications (e.g. [15–20]).

The benefits of MTDSC technique have been documented in several recent papers [21–26]. One of the most important benefits is the separation of complex transitions such as the glass transition into more easily interpreted components [26, 27]. In conventional thermal analysis, the sample temperature is either ramped

linearly at a constant heating or cooling rate (r or q respectively) or kept constant (as in isothermal experiments). In MTDSC, the sample temperature is modulated sinusoidally about a constant ramp so that the temperature T at time t is

$$T = T_0 + rt + A\sin\left(\frac{2\pi t}{P}\right)$$

where T_0 is the initial (or starting) temperature, r is the heating rate (which may also be a cooling ramp, q), A is the amplitude of the modulation and P is the period. The resulting instantaneous heating rate, $\mathrm{d}T/\mathrm{d}t$, therefore varies sinusoidally about the average heating rate r. The apparatus measures the amplitude of the instantaneous heat flow and the average heat flow, called the total heat flow and denoted by HF, and then by carrying out a suitable Fourier deconvolution of the measured quantities (also incorporating the sinusoidal temperature signal) it determines two quantities:
(a) Reversing heat flow (RHF)*
(b) Nonreversing heat flow (NHF)

The average heat flow which corresponds to the average heating rate (r) is called the total heat flow (HF). Total heat flow is the only quantity that is available and hence it is the only quantity that is always measured in conventional DSC experiments. Reversing heat flow RHF is that component of heat flow in the MTDSC that is *in phase* with the instantaneous heating rate, i.e.

$$\mathrm{RHF} = \left(\frac{\mathrm{d}Q}{\mathrm{d}t}\right)_{\mathrm{Reversing}} = \mathrm{C}_p\left(\frac{\mathrm{d}T}{\mathrm{d}t}\right)$$

The nonreversing heat flow is difference between the total heat flow and the reversing heat flow and represents heat flow due to a kinetically retarded process such as crystallization. No such information could be determined hitherto with previous conventional thermal instruments and from this perspective the apparatus is a unique and powerful tool that can separate heat flow into its reversing and nonreversing components. Heat capacity measurements by conventional DSC experiments therefore represent an "apparent", "total" or "average" heat capacity. In contrast, heat capacity measurements by MDSC represent heat capacity that is associated with a reversing heat flow only over the time scale of the experiment, which is the period P of the oscillations, and hence represents what we intuitively associate with the interpretation of heat capacity. This heat capacity has been called the "reversing heat capacity". In the glass transition region, the reversing heat capacity is approximately the same as storage heat capacity, that is the real part of the complex heat capacity [28]. In the last few years, the MTDSC technique has been already applied to the study of glass transition in a number of amorphous polymers (e.g. [21, 26, 27]) that exhibit an endothermic relaxation peak. The reversing heat flow through the T_g region exhibits a step change and represents the change in the heat capacity. The location of this change depends on the oscillation period [27, 29]. Hysteresis effects associated with thermal history are absent in the RHF but present in the NHF. The interpretation of the NHF has been more difficult but it is believed that it provides an indication of the enthalpy loss during the annealing period below T_g [26] though more research is needed to clarify its interpretation. It should be mentioned that MTDSC is not an ac calorimeter inasmuch as it measures both reversing and nonreversing heat flows. Detailed interpretations of reversing and nonreversing heat flows in MTDSC experiments, and their significance, are still a subject of lively topical discussion s in the literature (e.g. [26, 28, 30]).

* Reversing and nonreversing terms are used to distinguish these heat flows from thermodynamically reversible and irreversible heat flows.

2. Experimental procedure

As_xS_{100-x} glasses, where $x = 0$–42 at %, were prepared from the constituent pure elements. Arsenic and sulfur of purity 5N were weighed and placed in precleaned and outgassed (by heating under vacuum to 900 °C) quartz ampoules. The ampoules were evacuated to a pressure of 1×10^{-3} Pa for 30 minutes and then sealed. The synthesis was performed in a rocking furnace with the ampoules exposed to a temperature of 650 °C for 24 hours. The bulk samples were crushed into small pieces and immediately weighted into aluminum hermetic pans and then sealed. A typical sample weight was of 18 to 20 mg.

The differential scanning calorimetry experiments were performed on a temperature-modulated DSC (MDSC™, model 2910, TA Instrument Inc., USA) using a liquid nitrogen cooling accessory and a nitrogen gas DSC cell purge. The instrument was calibrated for enthalpy, temperature readings and specific heat capacity (C_p). An empty hermetic pan was the reference sample.

All samples in this work were given the same thermal history by heating to a temperature above the glass transition (at 20 °C/min), equilibrating and then cooling at a rate of 5 °C/min to a temperature of 20 °C.

The modulated-temperature DSC regime was used to measure the modulated heat flow in both heating and cooling schedules. The underlying heating and cooling rates were 5 °C/min, the oscillation amplitude was ±1.061 °C, and oscillation period was 80 seconds. The total heat flow, HF, reversing and non-reversing heat flows, RHF, NHF respectively, were deconvoluted from the modulated heat flow, MHF. The MHF signal and deconvoluted heat flows, HF, RHF and NHF, for glasses of composition $As_{40}S_{60}$ and $As_{16.6}S_{83.4}$ in both heating and cooling schedules are shown in Figs 1–4 as typical examples. The figures also illustrate the definitions of T_g and ΔH.

The structure of the bulk As_xS_{100-x} glasses were studied by Raman spectroscopy. Arsenic pentasulphide (As_2S_5) for the Raman structural study was prepared by precipitation from an acidified aqueous solution of Na_3AsS_4 [31]. The Raman spectroscopy study was performed on a Fourier Transformation (FT) Raman spectrometer model IFS/FRA 106, Bruker. Raman spectra were excited using a laser beam with $\lambda = 1064$ nm

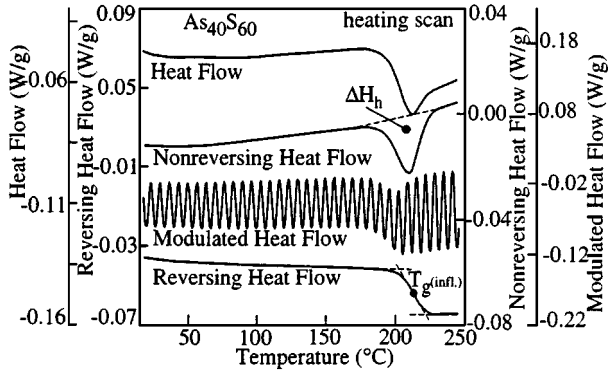

Figure 1 Typical conventional DSC (HF) and MTDSC (MHF, NHF and RHF) results during a heating scan. NHF shows a relaxation peak which is separated out from MHF using RHF. HF is the average heat flow, MHF is the modulated or instantaneous heat flow, NHF is the non reversible heat flow and RHF is the reversible heat flow.

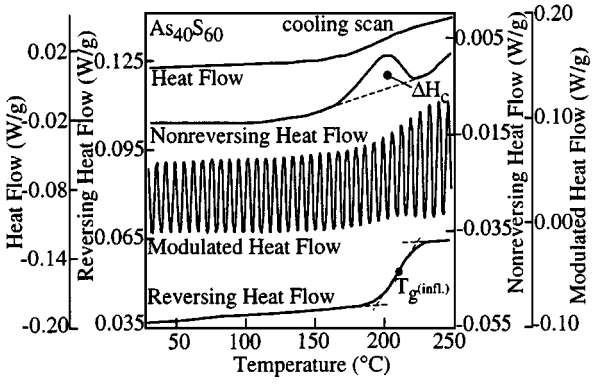

Figure 2 Typical conventional DSC (HF) and MTDSC (MHF, NHF and RHF) results during a cooling scan. NHF shows a relaxation peak which is separated out from MHF by subtracting RHF.

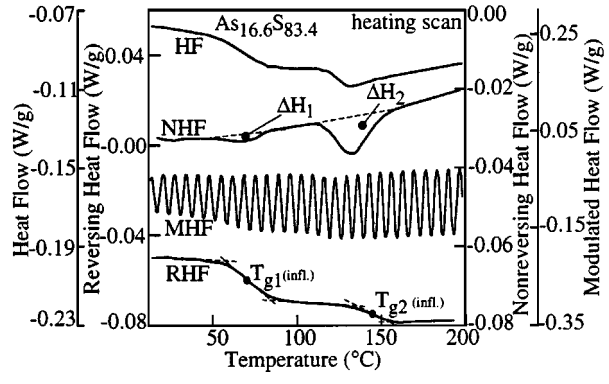

Figure 3 Typical conventional DSC (HF) and MTDSC (MHF, NHF and RHF) results during a heating scan for two phase As-S glasses. NHF shows a relaxation peak which is separated out from MHF using RHF. HF is the average heat flow, MHF is the modulated or instantaneous heat flow, NHF is the non reversible heat flow and RHF is the reversible heat flow.

having an output power 50 mW. The wavelength of the laser beam was critical to avoid any photostructural change in these chalcogenide glasses within the time scale of 100 scans. The resolution of the Raman spectrometer was 1 cm^{-1}.

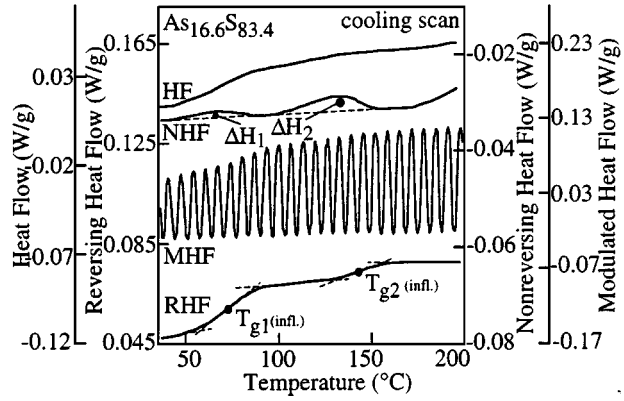

Figure 4 Typical conventional DSC (HF) and MDSC (MHF, NHF and RHF) results during a cooling scan for two phase As-S glasses. NHF shows a relaxation peak which is separated out from MHF by subtracting RHF.

3. Results

Fig. 5 shows the dependence of the glass transition temperature, T_g (infl.), on the composition of the As-S glass. There are various operational definitions of the glass transition temperature in the literature. A T_g-definition based on the change in the baseline of the reversing heat flow component in the glass transformation region during a cooling (or a heating scan) is shown in Figs 1–4. We note that the glass transition is exhibited as a change in the base line in the reversing heat flow i.e. change in heat capacity (as in the definition of T_g based on a second order transition). The glass transition temperature T_g (infl.) increases with increasing As concentration ($x \geq 25$ at %) up to a sharp maximum at 40 at % As (As_2S_3). T_g decreases with As content beyond 40 at % As. There appears to be a small change in T_g at 28 at % As, though this is small and not clearly

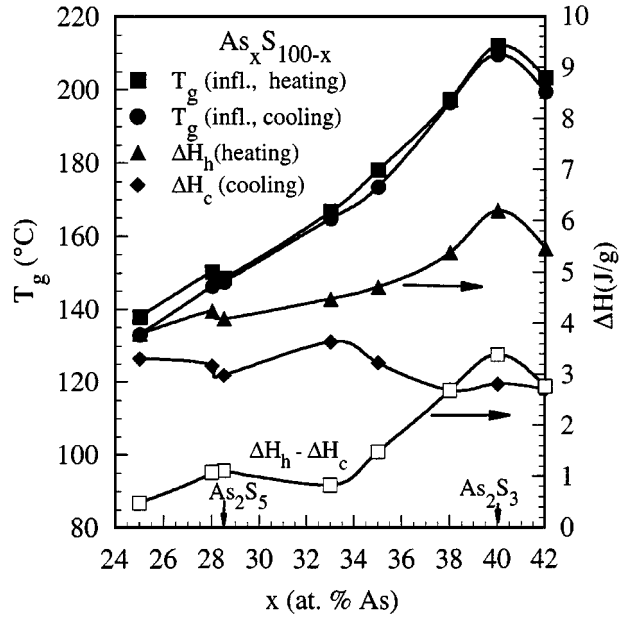

Figure 5 Glass transition temperature T_g and relaxation enthalpy ΔH vs. composition of the As-S glass system. Both structural parameters, T_g and ΔH are obtained from heating and cooling scans. The vertical arrows identify the critical compositions corresponding to stoichiometric compositions. ΔH axis is on the right whereas the T_g axis is on the left.

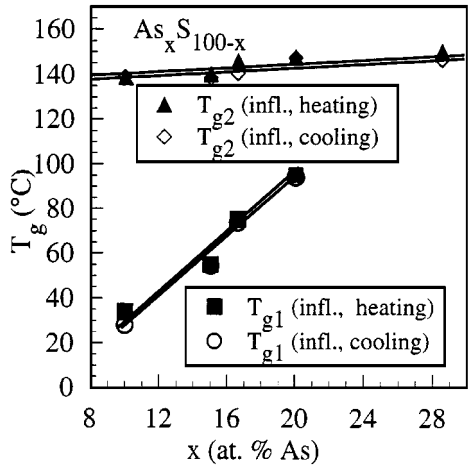

Figure 6 Glass transition temperature T_{g1} and T_{g2} vs. composition of the As-S glass system. The T_{g1} and T_{g2} are obtained from heating and cooling scans for two phase As-S glasses.

distinguishable from the rest of the T_g vs. composition behavior.

The MTDSC measurements show that the As_xS_{100-x} glasses, where $x < 25$ at % As, contain two glass phases, which are identified by the presence of two glass transition regions for both heating and cooling scans, as shown, for example, in Figs 3 and 4. While the low temperature glass transitions, T_{g1} (infl.), depend strongly on the As content, the high temperature glass transitions, T_{g2} (infl.), remain almost constant, as displayed in Fig. 6, and very close to the typical T_g value of the $As_{28.5}S_{81.5}$ glass.

Figs 5 and 7 also show the compositional dependence of the relaxation enthalpies ΔH, ΔH_1 and ΔH_2, respectively, for the As-S glasses during the glass transition. ΔH was found by integrating the non-reversing heat flow (NHF) in heating scans as shown in Figs 1–4. If the ultimate interest is constructing a correlation curve for comparing the area of the relaxation endoterm with other "end-use" properties, then the error in non-reversing heat flow curve can be ignored because the same modulation period is used. To obtain an absolute measure of the heat of relaxation ΔH, we have to subtract the relaxation enthalpy (ΔH_c) obtained during the cooling scan from the relaxation enthalpy (ΔH_h) obtained during the heating scan as demonstrated for polyethylene [32]. The compositional dependence of ΔH ($\Delta H = \Delta H_h - \Delta H_c$) has a behavior similar to that of the glass transition temperature with a similar distinct maximum at 40 at % As. As above, there appears to relatively small local minor peak at 28.5 at % As (As_2S_5) which is more pronounced than that in the T_g-x behavior above. Two phase As-S glasses ($x < 25$ at % As) are characterized by two relaxation enthalpies ΔH_1 and ΔH_2. The ΔH_1 vs. composition behavior exhibits a minimum at $As_{16.6}S_{83.4}$ i.e. (As_2S_{10}), ΔH_2 decreases with increasing As content towards the $As_{10}S_{90}$ glass as shown in Fig. 7. For each composition we carried out several experiments and all showed good reproducibility. The experimental points represent average values with typical error bars comparable with the size of the plotted experimental point. The smooth curves in Fig. 7 are spline curve fits to the data.

The specific heat capacities (C_p) of As-S glasses were measured by MTDSC in both heating and cooling scans. The C_p determination uses the reversing heat flow. This C_p is the heat capacity over the time scale of the experiment (oscillation period) as defined by Reading [1]. A typical result for a glass of the composition $As_{40}S_{60}$ is shown in Fig. 8. The glass transition is reflected as a step-like change in the C_p vs T behavior. The As-S glasses with two glass phases contain two heat capacity step changes occurring in the two glass transition regions, as shown in Fig. 9. The dependences of C_p, C_{p1} and C_{p2} (defined in Figs 8 and 9) on the As-S glass composition at the temperature $T_r = 0.9T_g$ are plotted in Fig. 10. The C_p vs. composition plot in Fig. 10 reveals a minimum 40 at % As. There is a small local threshold at about 28 at % As. There is also an unusual minimum in C_p in Fig. 10 at about 34 at % which does not occur in other properties, as discussed below, and is absent in As-Se glasses [2]. While C_{p1} increases with the As content in Fig. 11, C_{p2} remains relatively constant as shown in Fig. 12. The compositional dependences of C_{p1} and

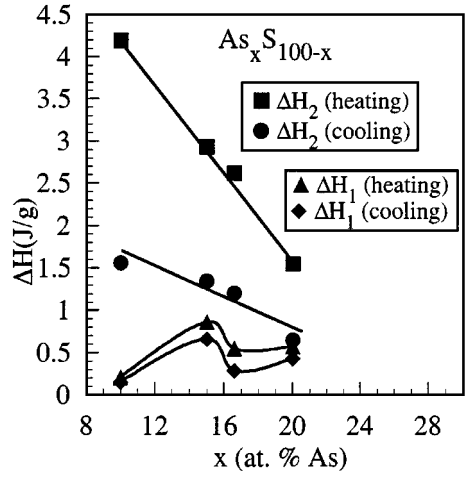

Figure 7 Relaxation enthalpy ΔH_1 and ΔH_2 vs. composition of the As-S glass system. The ΔH_1 and ΔH_2 are obtained from heating and cooling scans for two phase As-S glasses.

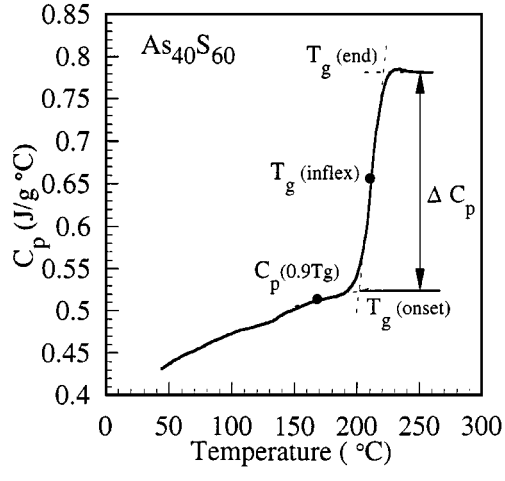

Figure 8 Typical specific heat capacity vs. temperature behavior in the glass transition region obtained from the RHF component of a MTDSC experiment during heating.

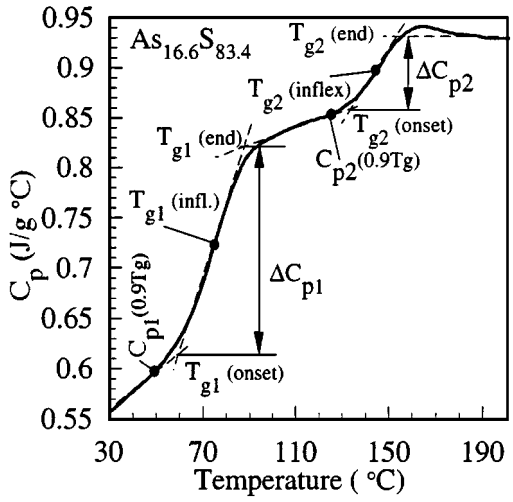

Figure 9 Typical specific heat capacity vs. temperature behavior in the glass transition region obtained from the RHF component of a MTDSC experiment during heating for two phase As-S glasses.

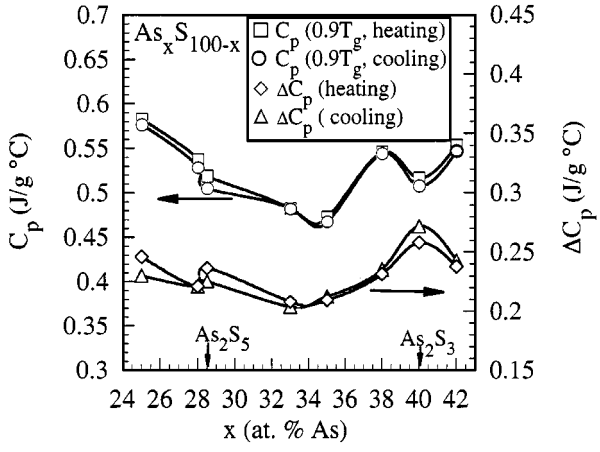

Figure 10 Specific heat capacity vs. composition for the As-S glass system. C_p values are taken at a temperature of $T_r = 0.9T_g$. Change in the specific heat capacity at the glass transition region plotted as a function of composition obtained from both heating and cooling scans during MTDSC experiments.

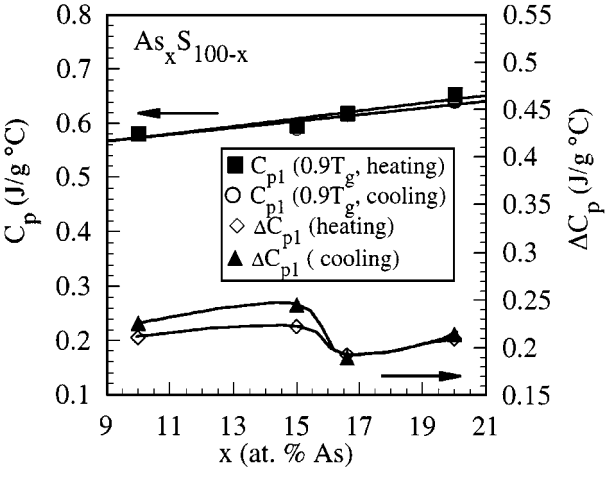

Figure 11 Specific heat capacity vs. composition for the As-S glass two phase system (phase 1). C_{p1} values are taken at a temperature of $T_r = 0.9T_{g1}$. Change in the specific heat capacity ΔC_{p1} at the glass transition region plotted as a function of composition obtained from both heating and cooling scans during MTDSC experiments.

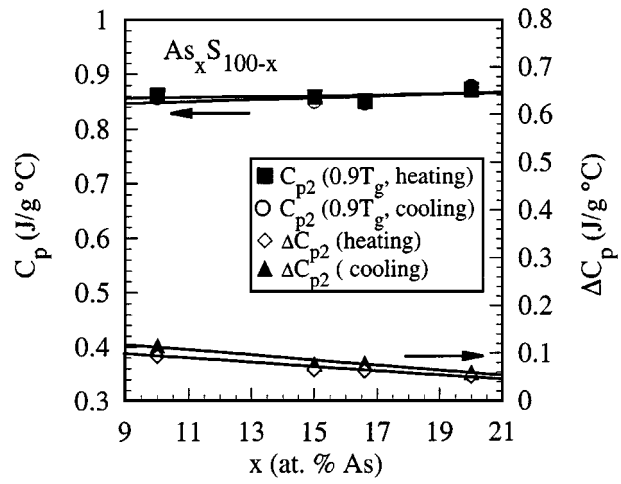

Figure 12 Specific heat capacity vs. composition for the As-S glass two phase system (phase 2). C_{p2} values are taken at a temperature of $T_r = 0.9T_{g2}$. Change in the specific heat capacity ΔC_{p2} at the glass transition region plotted as a function of composition obtained from both heating and cooling scans during MTDSC experiments.

C_{p2} are similar to those of T_{g1} and T_{g2}, respectively. In general, C_p measurements by MTDSC typically have reproducibilities better than ±1% [33].

The specific heat capacity differences ΔC_p, ΔC_{p1} and ΔC_{p2} in the glass transition region (sometimes called "configurational heat capacity") were determined for all the As-S glass compositions as illustrated in Figs 8 and 9. These are plotted as a function of composition in Figs 10–12. The ΔC_p vs. composition behavior exhibits a clear maximum at 40 at % As. There is a small local maximum in ΔC_p behavior (Fig. 10) at 28.5 at % As. There is obviously a "valley" between the two peaks (as expected) but without a distinct feature that corresponds to 34 at % As as for the C_p behavior. There are no special features in the ΔC_{p2} vs. composition behavior (which occurs for $x < 28.5$ at % As). The ΔC_{p1}, on the other hand, reveals a significant change around the composition $As_{16.6}S_{83.4}$.

The results of Raman spectroscopy studies in the As_xS_{100-x} glasses are shown in Fig. 13. The $As_{42}S_{58}$ glass (Fig. 13, curve a) contains strong bands at 345 and 362 cm^{-1} and multiple weak bands in the spectral region 100–300 cm^{-1}.

The dominant feature of the $As_{40}S_{60}$ bulk glass (Fig. 13, curve b) is a strong band at 343 cm^{-1}. There are also detectable weak bands at 168, 189, 222, 236 and 494 cm^{-1}. The Raman spectra of the $As_{28.5}S_{71.5}$ glass (composition equivalent to stoichiometric As_2S_5) and As_2S_5 precipitate with characteristic bands at 219, 236, 336, 365, 469, 474 and 494 cm^{-1} do not show any significant differences; these are shown in Fig. 13 as curves d and e, respectively. The As_xS_{100-x} glasses with $x < 28$ at % As contain the characteristic bands 153, 219 and 474 cm^{-1} whose intensity increases with the S-content. The same glasses also have the characteristic bands 336 and 365 cm^{-1} whose intensity, on the other hand, decreases with the S-content.

4. Discussion

The T_g values measured in this works are defined in terms of the reversing heat flow component and, further,

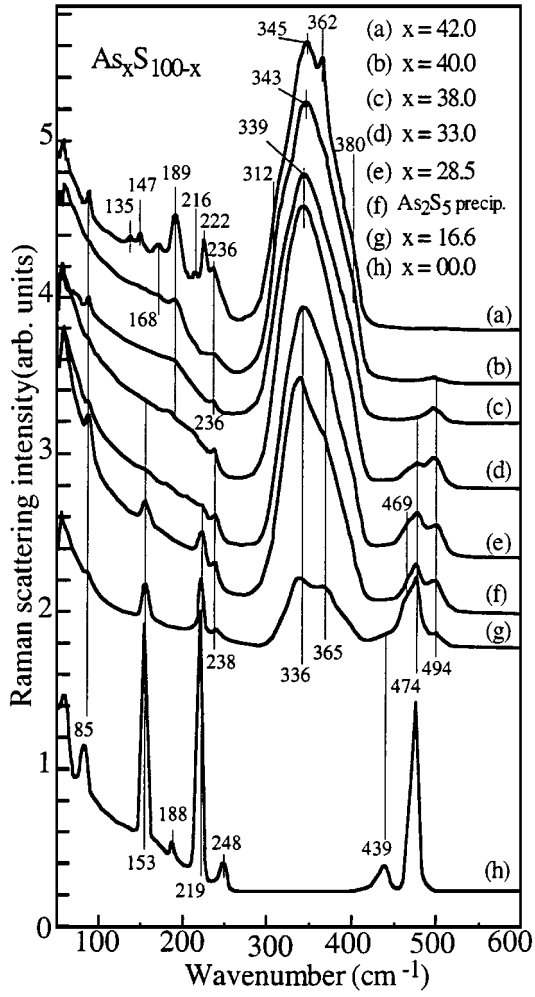

Figure 13 Raman spectra of the As_xS_{100-x} glasses and As_2S_5 precipitate.

we report T_g values determined from heating as well as cooling scans on samples that have the same thermal history. The T_g values reported previously from conventional DSC data (e.g. [31, 34] agree, in general trend and in the location of the maximum at 40 at % As, with our MTDSC data. The T_g results in this work however point to a small local threshold at 28.5 at % when we consider all the MTDSC results in entirety. Although, further experiments with closer compositions are required to unambiguously demonstrate this small threshold behavior in T_g, its simultaneous occurrence in C_p and ΔC_p vs composition curves gives support for this threshold at 28.5 at % As which corresponds to As_2S_5. Furthermore, there is a similar but a clear (large) extremum at the same composition in the same thermal properties in the analogous As_xSe_{100-x} glasses as reported previously [2]. No such features were observable in Te_xSe_{100-x} chalcogenide glasses (studied in this laboratory) where one element simply substitutes for another without a change in the structure [3].

Extrema and thresholds in various physical properties occur when there are distinct changes in the glass structure as discussed by a number of authors (e.g. [8–11]). The threshold behavior (or extrema) in various physical properties when the average coordination number Z in the glass network reaches 2.4 is now well documented [8–11] and corresponds to the large extrema we have observed at the composition 40% at As. At this mean coordination number the glass structure has the optimal network topology. However, the glass structure can also have a degree of medium range order, and contain various connected clusters or distinct structural units, whose difficult identification has been a topical subject of discussion in the literature (e.g. [13, 35, 36]). If one can argue that the glass structure will be more stable at certain compositions due to the presence of a distinct medium range order or the presence of certain distinct molecular units, then it would be reasonable to expect thresholds in certain properties of the glass, though the magnitude of the changes is unlikely to be as large as those at $Z = 2.4$. We believe that threshold at 28.5 at % As probably represents a distinct structure that corresponds to As_2S_5 which is discussed with the Raman results below.

MTDSC experiments clearly indicate a glass phase separation in As-S glasses. The power of the MTDSC technique is apparent when we compare the two clearly discernable T_g transitions in the RHF curve (the reversing heat flow) with the HF (total heat flow) curve in Fig. 4. In normal DSC experiments, only the latter would be available. We believe that the nearly constant value of T_{g2} close to the characteristic T_g value for $As_{28.5}S_{81.5}$ (As_2S_5) glass is a good indication of the similarity of the structure of the $As_{28.5}S_{81.5}$ (As_2S_5) glass and the structure of the high temperature glass phase in the As_xS_{100-x} glasses with $x < 25$ at % As. Further supporting evidence for the distinct $As_{28.5}S_{81.5}$ (As_2S_5) structure in the glass is that the C_{p2} value is constant and that ΔC_{p2} of the high temperature glass phase decreases monotonically with As content ($x < 25$ at % As) without any characteristic features (maxima or minima). Based on the compositional dependence of T_g, we believe that the high temperature glass phase keeps the same composition and structure as the $As_{28.5}S_{81.5}$ (As_2S_5) glass.

The structure of As_xS_{100-x} glasses was studied by Raman spectroscopy as shown in Figure 13 and spectra were interpreted using references [37–41]. The dominant feature of the $As_{40}S_{60}$ and $As_{42}S_{58}$ bulk glasses is the $AsS_{3/2}$ pyramidal unit (strong band at 343 cm^{-1} and 345 cm^{-1}). The symmetric stretching vibrations of AsS_3 pyramids are responsible for the presence of the most intense broad band between 300–400 cm^{-1} with a maximum at about 343 cm^{-1}. This strong band is partially deformed by weaker overlapped bands at 312, 362 and 380 cm^{-1}. The bands at 312 and 380 cm^{-1} are believed to be assigned to interactions among the AsS_3 pyramids. The band at 362 cm^{-1}, which corresponds to the vibration of As_4S_4 structural units, is quite strong in As rich glassy samples ($x > 40$ at %).

Beside this dominant broad band, there is a group of closely spaced narrow bands in the spectral region between 125–260 cm^{-1} in the spectrum of As rich glasses, where $x > 40$ at % As. These bands are of very low intensity in $As_{40}S_{60}$ glass and bellow the detection limit of Raman spectroscopy in S rich glasses. Similar bands at 145–147, 168–170, 187–191 and 218–222 and 231–236 cm^{-1} have been found by many authors [39–43] in As_4S_4 crystals and assigned to As-As vibrations.

Strong bands at about 335–345 cm^{-1} appear for the structure of glasses in the compositional region $28.5 < x < 40$ at %. These are believed to be due to pyramidal units AsS_3 with extra sulfur atoms incorporated into the (–S–S–) chains linking the pyramidal units together. The AsS_3 remains as a basic unit even in this part of the compositional region.

The three bands 153, 219 and 470 cm^{-1} associated with S_8 rings in the pure S spectrum decrease in magnitude due to disappearance of S_8 ring or ring-like (i.e. ring-fragments) structures as S is alloyed with As.

According to the Raman spectra, the structure of the $As_{28.5}S_{71.5}$ glass has a distinct character and this structure is very similar to that of the As_2S_5 precipitate as shown in Fig. 13. The structural unit responsible for bands at 336 and 365 cm^{-1} has not been fully elucidated as discussed in the literature [44, 45]. The structure of As_2S_5 can be interpreted, for example, through polymericaly linked $S = AsS_{3/2}$ (band 365 cm^{-1}) structural units, a structure made up of pyramidal $AsS_{3/2}$ (336 cm^{-1}) units interconnected by S–S chains (494 cm^{-1}), or a dynamic equilibrium between both structures as illustrated in Fig. 14. Raman spectrum shows an additional line at 469 cm^{-1}, which according to Dienmann [44], should be due to an As-S stretching mode of a terminal, i.e. nonbridging, arsenic sulfur bond. Although the As-S phase diagram does not indicate the formation of As_2S_5 as a definite compound in Fig. 15, the As_2S_5 has been reported as a crystalline compound by Borisova [46]. According to Barisova, the As_2S_5 crystals were crystallized from As_2S_5 glass at 250 °C in a pressure interval from 50 to 70 kbar. The XPA analysis in reference [46] was able to show that it is a separate chemical compound with melting point 190 °C and with a rhombic symmetry.

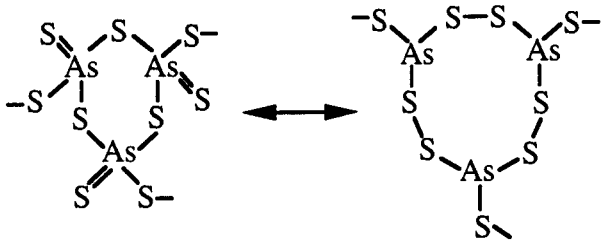

Figure 14 Proposed building blocks of As_2S_5 structure.

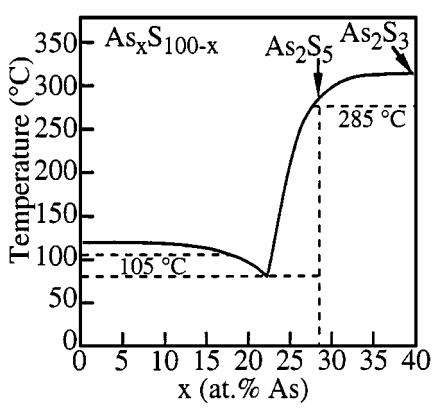

Figure 15 Phase diagram of the As-S system [46].

As_2S_5 has been also obtained as an amorphous compound (glass or precipitate). A comparison of the Raman spectra of the As_2S_5 glass and amorphous As_2S_5 deposits precipitated by hydrochloric acid from an Na_3AsS_4 solution at 0 °C indicates that molecular vibration bands are largely similar in the As_2S_5 glass and precipitate. According to Diemann [44] vibrational and photoelectron spectroscopic investigations as well as radial distribution curve indicate $S = AsS_{3/2}$ short range order. Each As-atom is connected to the bridging S-atoms at a distance of 230 pm and one terminal S-atom at 212 pm.

5. Conclusions

The modulated-temperature differential scanning calorimetry technique (MTDSC) was used to characterize the thermal properties of As_xS_{100-x} glasses in the glass transition temperature region. The structurally determined parameters T_g, ΔH, C_p and ΔC_p, obtained from reversing and nonreversing heat flow components during cooling and heating MTDSC scans, reveal extrema when the As-S glass system reaches the stoichiometric composition at 40 at % As (As_2S_3) which corresponds to the optimal coordination number 2.4. In addition, when we consider all the MTDSC results in entirety, that is T_g, C_p, ΔC_p and ΔH vs. composition behaviors, there is a relatively small but consistent threshold at about 28.5 at % As (As_2S_3). This threshold was not as clear as that reported As_xS_{100-x} glasses but we believe that it is due to a distinct structure. It was shown that As_xS_{100-x} glasses where $x < 25$ at % As are formed from two glass phases. From MTDSC measurements, it was possible to establish the probable composition of the high temperature glass phase and, further, by using Raman spectroscopy it was possible to correlate the MTDSC results with the structure of the As-S glasses. Our experimental results give support to glass structure theories that have been used in the interpretation of the compositional dependence of various physical properties, such as the Phillips-Thorpe topological models (major extrema at 40 at % As), and models that claim a degree of chemical ordering (small extrema at 28.5 at % As).

Acknowledgements

The authors thanks NSERC (Canada) for providing financial support for this project. One of the authors (TW) thanks NATO for an international research fellowship tenured between 1995–1997 at the University of Saskatchewan in Canada.

References

1. M. READING, D. ELLIOTT and V. L. HILL, *J. Thermal Analysis* **40** (1993) 949.
2. T. WAGNER and S. O. KASAP, *Philos. Mag. B* **74** (1996) 667.
3. S. O. KASAP, T. WAGNER and K. MAEDA, *Jpn. J. Appl. Phys.* **35** (1996) L1116.
4. T. WAGNER, S. O. KASAP and K. MAEDA, *J. Mater. Res.* **12** (1997) 1893.
5. X. FENG, W. J. BRESSER and P. BOOLCHAND, *Phys. Rev. Letts* **78** (1997) 4422.

6. X. FENG, W. J. BRESSER, M. ZHANG, B. GOODMAN and P. BOOLCHAND, *J. Non-Cryst. Solids* **222** (1997) 137.
7. T. WAGNER, S. O. KASAP and K. PETKOV, *J. Mater. Sci.* **32** (1997) 5889.
8. J. C. PHILLIPS, *J. Non-Cryst. Solids* **34** (1979) 153.
9. *idem.*, *Physics Today*, February (1982) 27.
10. M. F. THORPE, *J. Non-Cryst. Solids* **57** (1983) 355.
11. K. TANAKA, *Phys. Rev. B* **39** (1989) 1270.
12. S. R. ELLIOTT, "Physics of Amorphous Materials" (Longman, New York, 1983) p. 53.
13. *idem.*, *Nature* **354** (1991), 445 and references therein.
14. M. T. MORA in "Amorphous Insulators and Semiconductors," edited by M. F. Thorpe and M. I. Mitkova (Kluwer Academic Publishers, Boston, 1996) p. 45.
15. K. TANAKA and H. HISAKUNI, *J. Non-Cryst. Solids* **198–200** (1996) 714.
16. H. HAMANAKA, S. KONAGAI, K. MURAYAMA, M. YAMAGUCHI and K. MORIGAKI, *ibid.* **198–200** (1996) 808.
17. T. WAGNER, V. PERINA, M. VLCEK, M. FRUMAR, E. RAUHALA, J. SAARILAHTI and P. J. S. EWEN, *ibid.* **212** (1997) 157.
18. N. P. EISENBERG, M. MANEVICH, M. KLEBANOV, V. LYUBIN and S. SHUTINA, *ibid.* **198–200** (1996) 766.
19. N. NORDMAN and O. NORDMAN, *J. Appl. Phys.* **82** (1997) 1521.
20. M. I. MITKOVA in "Amorphous Insulators and Semiconductors," edited by M. F. Thorpe and M. I. Mitkova (Kluwer Academic Publishers, Boston, 1996) p. 71.
21. M. READING, A. LUGET and R. WILSON, *Thermochimica Acta* **238** (1994) 295.
22. B. WUNDERLICH, Y. JIN and A. BOLLER, *ibid.* **238** (1994) 277.
23. S. SAUERBRUNN and L. THOMAS, *American Laboratory* January (1995) 19.
24. L. THOMAS, "NATAS Notes," Vol. 26 (North American Thermal Analysis Society, Sacramento, CA, USA,1995) p. 48.
25. B. HASSEL, "NATAS Notes" Vol. 26 (North American Thermal Analysis Society, USA) **26** (1995) p. 54.
26. K. J. JONES, I. KINSHOTT, M. READING, A. A. LACEY, C. NIKOLOPOULOS and H. M. POLLOCK, *Thermochim. Acta* **304** (1997) 187.
27. A. BOLLER, C. SCHICK and B. WUNDERLICH B, *ibid.* **266** (1995) 97
28. J. M. HUTCHINSON and S. MONTSERRA, *ibid.* **304** (1997) 257.
29. *idem.*, *ibid.* **286** (1996) 263.
30. J. E. K. SCHAWE, *ibid.* **261** (1995) 183.
31. A. FELTZ, "Amorphous Inorganic Materials and Glasses" (VCH, Weinheim, 1993) Chaps. 2 and 3, p. 16, 212 and references therein.
32. "Modulated DSCTM Compendium, Basic Theory and Experimental Considerations," TA Instruments (TA Instruments Inc., Newcastle, DE, USA, 1996) pp. 25–27.
33. P. S. GILL, S. R. SAUERBRUNN and M. READING, *J. Thermal Analysis* **40** (1993) 931.
34. R. BLACHNIK and A. HOPPE, *J. Non-Cryst. Solids* **34** (1979) 191.
35. J. C. PHILLIPS, *ibid.* **43** (1981) 37.
36. A. FELTZ, "Amorphous Inorganic Materials and Glasses" (VCH, Weinheim, 1993) Chap. 3.
37. A. T. WARD, *J. Physical Chemistry* **72** (1968) 4133.
38. P. J. S. EWEN, M. J. SILK and A. E. OWEN, "The Structure of Non-Crystalline Materials," edited by P. H. Gaskell (Taylor and Francis, London, 1977) p. 127.
39. G. LUCOVSKY, F. L. GEILS and R. C. KEEZER, "The Structure of Non-Crystalline Materials," edited by P. H. Gaskell (Taylor and Francis, London, 1977) p. 127.
40. O. I. SHPOTYUK, *Zh. Prikl. Spektroskopii* **59** (1993) 551.
41. O. I. SPOTYUK, *Phys. Stat. Sol. B* **183** (1994) 365.
42. S. A. SOLIN and G. V. PAPATHEODOROU, *Phys. Rev. B* **15** (1997) 2087.
43. M. FRUMAR, A. P. FIRTH and A. E. OWEN, *Philos. Mag. B* **50** (1984) 463.
44. E. DIEMANN, *Revue de Chimie Minerale* **16** (1979) 237.
45. A. FELTZ and G. PFAFF, *J. Non-Cryst. Solids* **77–78** (1985) 1137.
46. Z. U. BORISOVA, "Glassy Semiconductor" (Plenum Press, New York, 1981) Chap. 2 and references therein.

Received 21 July
and accepted 16 September 1998